

Nanofibers of polyaniline synthesized by interfacial polymerization

Xinyu Zhang^a, Roch Chan-Yu-King^b, Anil Jose^b, Sanjeev K. Manohar^{a,*}

^a Alan G. MacDiarmid Laboratory for Technical Innovation, Department of Chemistry, The University of Texas at Dallas, Richardson, TX 75083, USA

^b University of Science and Arts of Oklahoma, Chickasha, OK 73018-5322, USA

Received 5 December 2003; received in revised form 17 March 2004; accepted 29 March 2004

Available online 10 June 2004

Abstract

The average diameter of polyaniline nanofibers obtained by interfacial polymerization using a solution of aniline in toluene as the top organic phase and acidic ammonium peroxydisulfate as the bottom aqueous phase can be controlled by using surface active dopants and/or surfactants in the aqueous phase. The average diameter of polyaniline nanofibers doped with camphorsulfonic acid (CSA) synthesized by interfacial polymerization decreases when twin-tailed anionic surfactants, based on the *cis*-1,2-alkylethene sulfonate structure (alkyl = C₅H₁₁ or C₇H₁₃), are used. For example, the average diameter of polyaniline CSA nanofibers decreases in the order 48 nm (no surfactant) > 35 nm (C₅H₁₁-twin-tailed) > 28 nm (C₇H₁₃-twin-tailed). This effect is reversed in polyaniline nanofibers synthesized using 2-acrylamido-2-methyl-1-propanesulfonic acid (AMPSA) as the dopant, e.g., the average fiber diameter of polyaniline AMPSA increases in the order 23 nm (no surfactant) < 35 nm (C₅H₁₁-twin-tailed) < 55 nm (C₇H₁₃-twin-tailed). The doping percentage is reduced when surfactants are used although there is no significant change in the pressed-pellet room temperature 4-probe DC conductivity compared to conventional (single-phase) polyaniline-HCl ($\sigma \sim 1\text{--}5$ S/cm). Polyaniline nanofibers also show increased capacitance consistent with their high surface area, e.g., a capacitance value of 277 F/g was observed in nanofibers of polyaniline-AMPSA (23 nm average diameter) compared to 11 F/g in non-fibrillar polyaniline-AMPSA powder. Further optimization and surfactant structure–function evaluation is needed to uncover the mechanism associated with this phenomenon.

© 2004 Elsevier B.V. All rights reserved.

Keywords: Interfacial polymerization; Nanofibers; Polyaniline; AMPSA; CSA; Twin-tailed surfactants

1. Introduction

We describe the influence of dopants and surfactants on the morphology and related properties of polyaniline nanofibers synthesized by the recently reported interfacial polymerization method in which aniline is chemically oxidatively polymerized to polyaniline at the interface of two immiscible liquids [1]. Unlike conventional (single-phase) aqueous chemical oxidative polymerization, interfacial polymerization of aniline using organic dopants like camphorsulfonic acid (CSA) results in polyaniline powder with fibrillar morphology having average fiber diameters <100 nm.

Interfacial polymerization is the latest among a variety of approaches to chemically synthesize nanostructured electronic polymers [2]. These include the use of physical (insoluble) templates such as zeolites [3], opals [4] and controlled

pore-size membranes [5], etc., and chemical (soluble) templates such as surfactant micelles [6,7], emulsions [8–10] and polymers [11,12]. Recently, a “non-template” method has been described in which large organic dopant anions are used during the reaction [13–16]. These bulky organic anions are believed to have “surfactant-like” properties and form aggregates in solution which act as pseudo-templates for fibrillar polymer growth. Conducting polymer nanofibers and nanotubes with diameters in the range of 650–80 nm have been obtained using this approach. Nanofibers have also been reported during the electrochemical polymerization of aniline in the presence of sulfonated porphyrin aggregates [17].

Interfacial polymerization can therefore be regarded as a non-template approach in which high local concentrations of both monomer and dopant anions at the liquid–liquid interface might be expected to promote the formation of monomer–anion (or oligomer–anion) aggregates. These aggregates can act as nucleation sites for polymerization resulting in powders with fibrillar morphology. In this study, we describe the synthesis and characterization of

* Corresponding author. Tel.: +1-972-883-6536; fax: +1-972-883-6586.
E-mail address: sanjeev.manohar@utdallas.edu (S.K. Manohar).

polyaniline nanofibers using different dopants and/or surfactants in the aqueous phase. Also described is their aqueous electrochemistry including capacitive charge/discharge measurements which demonstrate their potential in energy storage applications.

2. Experimental

2.1. Materials

Aniline (99.5+%), ammonium peroxydisulfate (98%), 2-acrylamido-2-methyl-1-propanesulfonic acid (AMPSA), 10-camphorsulfonic acid (98%), dodecylbenzenesulfonic acid (DBSA), octylphenol ethoxylate Triton-X 100, sodium di(2-ethylhexyl) sulfosuccinate aerosol-OT (AOT), 1-methyl-2-pyrrolidinone, NMP (99%), toluene and acetonitrile were purchased from Sigma-Aldrich (Milwaukee, WI). The single-tailed non-ionic surfactant d-Alpha Tocopheryl Polyethylene Glycol 1000 Succinate (Vitamin E TPGS) was purchased from Eastman Chemical Company. The twin-tailed surfactants, potassium *cis*-1,2-dipentylethene sulfonate (C₅H₁₁-twin-tailed) and potassium *cis*-1,2-diheptylethene sulfonate (C₇H₁₃-twin-tailed) were synthesized in-house (see Table 1 for structure) [18].

2.2. Instrumentation and measurements

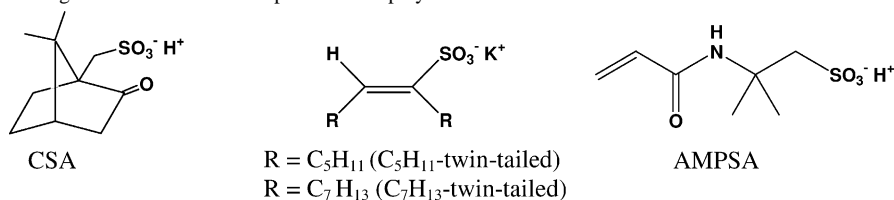
Cyclic voltammetry was carried out (Arbin Instruments, model MSTAT4+) in aq. 1.0 M CSA or HCl electrolyte by cycling the potential between -0.2 and 0.9 V (SCE reference) at 20 mV/s using Pt mesh as the working electrode and Pt wire as the counter electrode. Standard pre-equilibration procedures were followed [19]. Open-circuit potential (V_{oc})

measurements were made using Pt foil as the working electrode versus SCE reference.

Capacitance measurements were performed by first identifying the potential range 0.4 – 0.5 V as a representative non-Faradaic region in the cyclic voltammogram of polyaniline and the area under the current–voltage plot representing the charge (or discharge) capacity was continuously recorded. The working electrode was Pt mesh which was folded at the tip. Within the fold an accurately weighed amount of polyaniline nanofibers (~ 2 mg) was pressed using a spatula. In all other fashions the experiment was similar to cyclic voltammetry described above. Using the features available in the MSTAT4+ potentiostat, the charge and discharge cycles were simultaneously monitored and cumulatively added over a total of 50 cycles and plotted. This plot provides more information than the conventional “rectangular box” plots normally employed in capacitance measurements. The capacitance (F/g) was calculated using the formula: capacitance (F/g) = charge (Q)/voltage (V) = (Ah \times 3600)/(# cycles \times voltage range \times wt.) = (mAh \times 3.6)/(50 \times 0.1 V \times weight (g)).

Elemental analyses were performed by Atlantic Micro-lab, Inc. Prior to analysis, samples were heated to ~ 80 °C in a vacuum oven for 72 h. Scanning electron microscopy (SEM) images were obtained using a Leo 1530 VP Field Emission Scanning Electron Microscope. The average fiber diameter was estimated directly from the instrument software and confirmed by importing the image and the scale bar into an image editing software (MS Paint). Four lines were drawn from edge to edge across the image, diagonals (2), vertical (1) and horizontal (1). In all instances where the line intersected the fiber image, the edge-to-edge pixel counts were measured. An average of all such crossings provided an estimate of the average fiber diameter.

Table 1
Average fiber diameter and capacitance of polyaniline nanofibers



Dopant	Surfactant	Fiber diameter (nm)	Capacitance (F/g)
CSA	None	~ 48	65
CSA	Triton-X 100 (non-ionic)	~ 80	NA
CSA	Vitamin E TPGS (non-ionic)	~ 60	NA
CSA	DBSA (anionic)	~ 50	NA
CSA	AOT twin-tailed (anionic)	~ 30	NA
CSA	C ₅ H ₁₁ -twin-tailed (anionic)	~ 35	111
CSA	C ₇ H ₁₃ -twin-tailed (anionic)	~ 28	154
AMPSA	None	~ 23	277
AMPSA	C ₅ H ₁₁ -twin-tailed (anionic)	~ 39	55
AMPSA	C ₇ H ₁₃ -twin-tailed (anionic)	~ 53	96
AMPSA	None	Non-fibrillar ^a	11

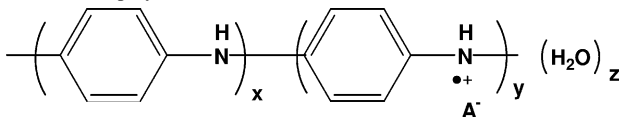
^a Obtained by destroying the fibrillar morphology of polyaniline-AMPSA nanofibers using the procedure outlined in Section 2.

Room temperature DC conductivity measurements were carried out using the standard 4-probe van-der Pauw method on compressed pellets (12 mm × 0.5 mm) made by placing ~150 mg sample in a stainless steel mould and applying a pressure of 6000 lb/cm² using a pellet press.

2.3. General synthesis

Ammonium peroxydisulfate (1.15 g) was dissolved in 200 ml of aq. 1.0 M solution of the dopant (AMPSA, CSA, etc.) in a 500 ml beaker. To this was added, gently and with minimal agitation along the sides of the beaker a solution of aniline (2 ml) in toluene (200 ml). The aniline/toluene solution forms the upper organic layer and the ammonium peroxydisulfate solution forms the lower aqueous layer. Immediately after the liquid–liquid interface is visible and is relatively free of agitation, surfactants (when used) were added to the aqueous phase in the following manner. Stock solutions (5 mg/ml) of C₅H₁₁-twin-tailed and C₇H₁₃-twin-tailed surfactants were prepared and 5 ml of this solution was gently syringed into the aqueous (bottom) layer just below the interface. The resulting two-phase system was covered with stretched parafilm or aluminum foil to minimize solvent evaporation and left undisturbed for ~12 h. As described in Fig. 1, during the very early stages of the reaction (~5 min), a gradual darkening could be observed at the interface followed by thin streams of dark blue-green material, presumably pernigraniline salt, sinking gradually into the aqueous phase (Fig. 1) [20]. When surfactants are used these streams form predominantly along the sides of the beaker, caused probably by the surfactant crowding out the monomer at the interface and forcing it to the edge of the beaker. After ~12 h, the reaction mixture was suction filtered and the dark green precipitate washed repeatedly with water (3 × 250 ml) and acetone (10 × 25 ml) until the acetone washings were colorless. The resulting bright green precipitate of polyaniline nanofibers was stirred overnight in aq. 1.0 M solution of the dopant (AMPSA, CSA, etc.), suction filtered, and washed with acetone (10 × 25 ml) to remove any excess dopant adhering to the precipitate. Drying under dynamic vacuum at 80 °C for ~12 h yielded doped polyaniline displaying a 4-probe pressed-pellet conductivity in the range $\sigma_{DC} \sim 1\text{--}5\text{ S/cm}$.

Table 2

Structure of polyaniline nanofibers^a


A	Surfactant	x	y	z
CSA	None	0.55	0.45	0.39
CSA	C ₅ H ₁₁ -twin-tailed	0.71	0.29	0.61
CSA	C ₇ H ₁₃ -twin-tailed	0.70	0.30	0.68
AMPSA	None	0.70	0.30	0.66
AMPSA	C ₅ H ₁₁ -twin-tailed	0.79	0.21	0.80
AMPSA	C ₇ H ₁₃ -twin-tailed	0.76	0.24	0.66

^a Structure estimated from the elemental composition (see Section 2).

Elemental analyses of polyaniline-CSA; theoretical values for the emeraldine oxidation state—C: 64.23; H: 5.60; N: 6.81; O: 15.57; S: 7.79; Total: 100.00. Found—C: 62.65; H: 6.07; N: 6.85; O: 17.41; S: 7.15; Total: 100.13 (no surfactant). C: 63.37; H: 5.94; N: 7.85; O: 16.62; S: 5.46; Total: 99.24 (C₅H₁₁-twin-tailed added). C: 62.98; H: 5.75; N: 7.61; O: 17.28; S: 5.52; Total: 99.14 (C₇H₁₃-twin-tailed added). See Table 2 for structure derived from the elemental analysis.

Elemental analyses of polyaniline-AMPSA; theoretical values for the emeraldine oxidation state—C: 58.76; H: 5.67; N: 10.82; O: 16.49; S: 8.25; Total: 100.00. Found—C: 59.31; H: 5.50; N: 11.14; O: 18.15; S: 5.88; Total: 99.98 (no surfactant). C: 61.99; H: 5.11; N: 10.39; O: 17.60; S: 4.50; Total: 99.59 (C₅H₁₁-twin-tailed added). C: 61.90; H: 5.19; N: 10.29; O: 16.86; S: 5.04; Total: 99.28 (C₇H₁₃-twin-tailed added). See Table 2 for structure derived from the elemental analysis.

Polyaniline with non-fibrillar morphology for use as controls in capacitance studies (Table 1) was obtained by first dedoping polyaniline-AMPSA nanofibers to the corresponding base form and dissolving it in NMP. Polyaniline base was then precipitated using a non-solvent, filtered, and redoped with AMPSA to obtain polyaniline-AMPSA powder with non-fibrillar morphology. 100 mg of polyaniline-AMPSA nanofibers was stirred in 11 aq. 0.1 M NH₄OH for ~12 h and the resulting black-brown powder of polyaniline base was suction filtered and dried under dynamic vacuum at

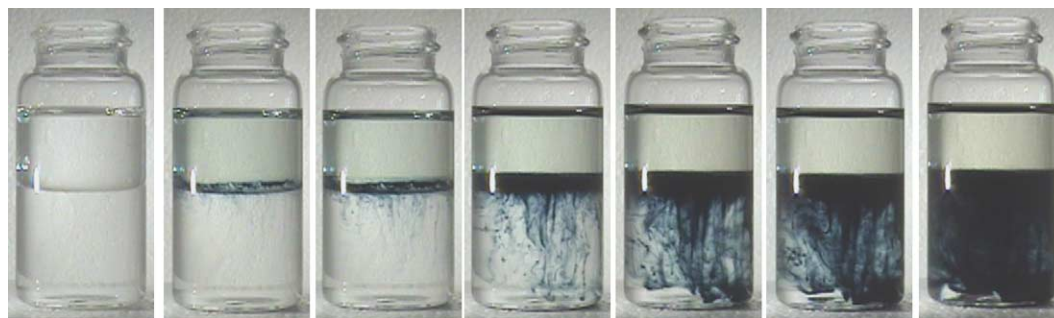


Fig. 1. Progress (from left to right) of a chemical oxidative interfacial polymerization of aniline using (NH₄)₂S₂O₈/aq. 1.0 M AMPSA as the bottom phase.

80 °C for ~12 h. A solution in NMP was made by adding the polyaniline powder, in ~10 mg quantities, to 10 ml NMP and stirring for 2 h to ensure complete dissolution. Forty milliliter of acetonitrile was added and stirred for ~1 h to precipitate the polyaniline base from solution (acetonitrile is a non-solvent for polyaniline base). The resulting bronze precipitate was suction filtered and redoped by suspending it in 1 l of a stirred solution of aq. 1.0 M AMPSA for ~12 h. Suction filtration and drying in the usual manner (described above) resulted in a bright green powder of non-fibrillar polyaniline-AMPSA (determined by SEM).

3. Results and discussion

A repeat of published work on the interfacial oxidative polymerization of aniline using a solution of aniline in toluene as the top organic phase and acidic ammonium peroxydisulfate as the bottom aqueous phase resulted in polyaniline-CSA nanofibers of average fiber diameter of ~48 nm (smallest ~30 nm; largest ~90 nm) consistent with the literature value of ~30–60 nm for average diameter [1]. Also, as described previously, when the reaction is carried out in the aqueous phase alone, i.e., a conventional one-phase synthesis, the precipitate of polyaniline-CSA obtained had non-fibrillar morphology. While reasons for the formation of nanofibers during interfacial polymerization are not clear, it appears that fibrillar growth is favored in systems in which: (a) the kinetics of monomer migration into the aqueous phase is significantly reduced, and (b) large soluble aggregates (monomer- or oligomer-based) are present at the interface. Compared to interfacial polymerization using aq. 1.0 M HCl, the onset of the reaction is significantly delayed when CSA is used. Just prior to the onset of the polymerization, one might anticipate the anilinium-CSA salt to accumulate at the interface and form larger aggregates as the interface becomes increasingly packed. We believe these aggregates could play an important role in orchestrating fibrillar polymer growth. We reasoned that any organic dopant possessing good interfacial packing properties should

help promote fibrillar morphology by both “a” and “b” above.

Indeed, when the reaction is carried out using aq. 1.0 M AMPSA as the aqueous phase, polyaniline-AMPSA nanofibers of average fiber diameter ~23 nm (smallest 14 nm; largest 40 nm) are obtained (Fig. 2, Table 1). The smaller average fiber diameter observed with AMPSA (versus CSA) is consistent with AMPSA’s more linear structure which might be expected to pack the interface more efficiently than CSA. There are two important points to note in these reactions: (a) the interface is not disturbed during the reaction (not stirred), and (b) the reaction is a precipitation polymerization, i.e., a precipitate forms almost immediately after the onset of polymerization. This precipitate, first observed as a thin greenish layer at the liquid–liquid interface, “grows” as more polymer is formed. Since this “early” precipitate is also expected to possess fibrillar morphology, surface active additives like surfactants, dopants, etc., could significantly affect fiber properties by influencing the kinetics of monomer migration across the interface by competing for the available and undisturbed interfacial area.

Using commercial non-ionic and anionic surfactants yielded the following results. Single-tailed non-ionic surfactants increase the average fiber diameter, e.g., both Triton-X 100 and Vitamin E TPGS increased the fiber diameter of polyaniline-CSA from ~50 to ~80 nm (Table 1). Conventional single-tailed anionic surfactants like DBSA not appear to have any significant impact on fiber diameter. Twin-tailed surfactants, however, seem to reduce fiber diameter, e.g., aerosol-OT (AOT) reduced the fiber diameter of polyaniline-CSA from ~50 to ~30 nm.

We then evaluated a largely unexplored class of surfactants based on the *cis*-1,2-dialkylethene sulfonate structure. We chose this family of twin-tailed surfactants since, to the best of our knowledge, this is the only class of surfactants that contain a central double bond that permanently separates the twin hydrophobic alkyl tails from the hydrophilic sulfonate head group (Table 1) [21]. When chemical oxidative interfacial polymerization is carried out with twin-tailed surfactants, the kinetics of initiation of the polymerization is

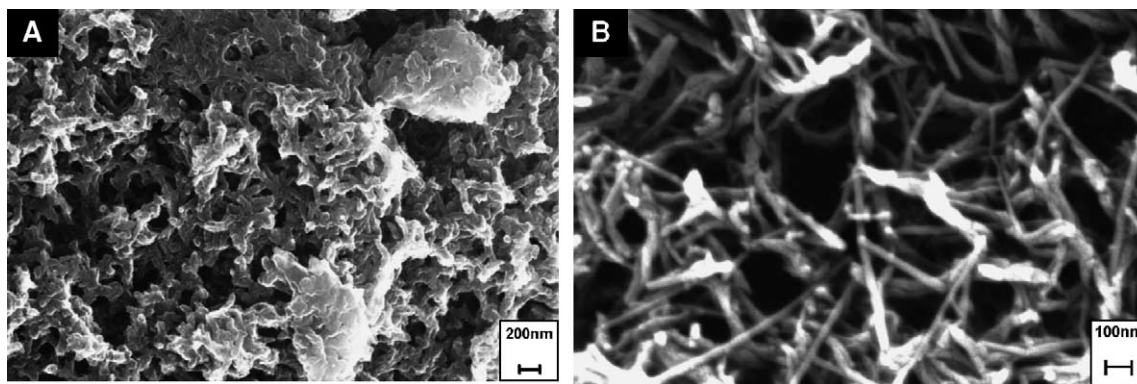


Fig. 2. SEM images of polyaniline-AMPSA powder synthesized by chemical oxidative polymerization: (A) conventional single-phase synthesis, (B) interfacial synthesis.

significantly reduced for it takes longer for the greenish layer to appear at the interface. Presumably, these surfactants help slow the kinetics of monomer migration to the interface.

The average fiber diameter of polyaniline-CSA nanofibers decreases as the surfactant alkyl chain length increases. For example, as described in Table 1 average fiber diameter *decreases* in the order 48 nm (no surfactant) > 35 nm (C₅H₁₁-twin-tailed) > 28 nm (C₇H₁₃-twin-tailed). However, in the case of polyaniline-AMPSA nanofibers, fiber diameter *increases* as the surfactant alkyl chain length increases in the order 23 nm (no surfactant) < 35 nm (C₅H₁₁-twin-tailed) < 55 nm (C₇H₁₃-twin-tailed). The reasons for the reversal in the trend are not clear at the present time although added surfactants might be expected to disrupt the intrinsic interfacial packing properties of AMPSA.

The mechanism of fibrillar morphology in interfacial polyaniline synthesis is reported to proceed by a monomer proximity effect where, unlike in conventional (single-phase) reactions, there is limited amount of aniline monomer in the vicinity of a growing polymer chain at the interface [1]. At the interface the growing polymer chain grows preferentially in a more ordered fashion, i.e., away from the interface resulting in fibrillar growth. In contrast, a growing polymer chain in a conventional single-phase reaction is surrounded by excess aniline monomer which can initiate random polymer growth resulting in disordered, particulate morphology. We believe that nanofibrillar morphology could also be related to aniline oligomers formed during the early stages of the reaction. These oligomers formed at the interface could promote fibrillar polymer morphology at the expense of particulate morphology. Indeed, there have been several reports on fibrillar morphology observed in polyaniline films synthesized by electrochemical polymerization of aniline in the presence of added aniline dimer, *N*-phenyl-1,4-phenylenediamine [22–24]. The addition of aniline dimer also lowered the oxidation potential of the system which was believed to produce more uniform polyaniline films of improved quality [24]. We believe that the formation and accumulation of aniline dimer at the interface could also promote fibrillar polymer growth by a similar mechanism. Dimer formation is also expected in conventional (single-phase) chemical oxidative polymerization of aniline, consistent with small amounts of nanofibrillar morphology observed in polyaniline-AMPSA (Fig. 2A). Any dimer formed in single-phase polymerization systems is quickly converted to longer chains due to efficient mixing of the contents of the reaction. In non-stirred, interfacial polymerization systems however, aniline dimer concentration is expected to steadily increase resulting in reaction conditions similar to previously reported electrochemical systems where aniline dimer was intentionally added [22–24]. Potential profiling of the interfacial polymerization of aniline also showed that the ‘plateau potential’, i.e. the highest V_{oc} of ~ 0.65 V (versus SCE) was lower than the value ~ 0.75 V (versus SCE) observed in single-phase polymerization of aniline [20] indicating that aniline dimer (or

oligomers) could indeed be present. Addition of surfactants to the interface is expected to affect the kinetics of dimer and oligomer formation at the interface (and their transport across it) which could play an important role in the morphology of the precipitate. Clearly, additional studies are necessary to confirm this mechanistic rationale.

The chemical structure of polyaniline nanofibers shown in Table 2 was derived from the elemental analyses described in the Section 2. The oxygen content appears to be significantly higher than the theoretical value for all samples synthesized by the interfacial polymerization route. These high oxygen values persist even when samples are heated at 100 °C for 24 h under dynamic vacuum. The absence of peaks related to carboxyl and/or carbonyl groups in the FT/IR and from the absence of spurious peaks in the cyclic voltammogram suggests the high oxygen content could be due to significant amount of tightly held water, either as water of hydration, or, should the fibers be hollow, as water trapped inside the fibers [25]. The doping percentage, as determined by the sulfur/nitrogen ratio decreases in the order 45% (no surfactant) < 29% (C₅H₁₁-twin-tailed) \sim 30% (C₇H₁₃-twin-tailed) for the polyaniline-CSA system (see ‘y’ value in Table 2). In addition, the low doping levels do not increase even after three redoping attempts, i.e., stirring overnight in aq. 1.0M CSA. The effect is more pronounced in the AMPSA system, i.e., even in the absence of added surfactants a low doping percentage of $\sim 30\%$ is observed in polyaniline-AMPSA nanofibers. This may be due to the intrinsic surface active properties of AMPSA. When surfactants are used, the doping percentage of the polyaniline-AMPSA system decreases even further, to $\sim 21\%$ (see ‘y’ value in Table 2). Low doping percentages observed do not appear to be related to average fiber diameter as described in Table 1 where both small and large diameter fibers show low doping percentages depending on the surfactant used.

The inability of lowly doped nanofibers to be fully doped by aq. 1.0M acids is consistent with: (a) the oxidative polymerization yielding polyaniline nanofibers with average oxidation state more reduced *or* more oxidized than the emeraldine oxidation state; or (b) incomplete protonic acid doping of the emeraldine oxidation state [26]. Considering that the reaction was carried out in air and the monomer/oxidant ratio was $\sim 4:1$, it appears unlikely that an oxidation state more reduced or more oxidized than the emeraldine oxidation state can be obtained for the parent polyaniline system under the experimental conditions. Electronic absorption spectra of solutions of the corresponding base forms in NMP indicate that the polymer is in the emeraldine oxidation state [27]. In addition, potential profiling of the reaction affords an open-circuit potential value $V_{oc} \sim 0.43$ V (versus SCE) at the end of the reaction which is also consistent with the polymer being present in the emeraldine oxidation state [7,20]. It is therefore not clear why low doping percentages are observed when surfactants are used, although one possible rationale involves extensive

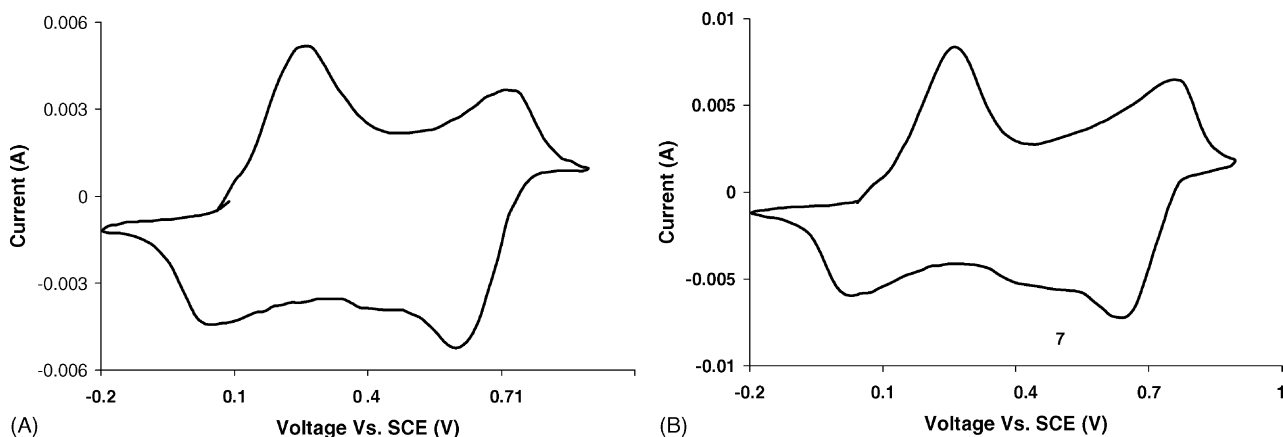


Fig. 3. Cyclic voltammograms of polyaniline-CSA powder in aq. 1.0M CSA electrolyte (SCE reference): (A) fibrillar morphology, average fiber diameter 28 nm; (B) non-fibrillar morphology.

phase segregation of the “bulk” emeraldine oxidation state into extended runs of fully reduced leucoemeraldine segments and fully oxidized pernigraniline segments [28]. Since only the “true” emeraldine segments can be doped, the total doping percentage is expected to be lower than 50%. Phase segregation of the emeraldine oxidation state has been previously observed in polyaniline films that display inconsistent electroluminescent behavior [28].

Aqueous electrochemistry is an important and sensitive tool to characterize doped polyaniline powder, e.g., cyclic voltammograms obtained in aq. 1.0M acids have helped determine its purity and identify structural defects along the polymer backbone [19]. The cyclic voltammograms of polyaniline nanofibers synthesized in this study show two redox peaks characteristic of the parent polyaniline system whose $E_{1/2}$ values are essentially identical conventional (non-fibrillar) emeraldine-CSA (Fig. 3). This suggests that not only are the nanofibers free of any backbone-related defects but that the aqueous electrochemistry of polyaniline,

at least in these instances, is not significantly affected by polymer morphology.

Previous studies on the electronic conductivity of polyaniline nanofibers obtained by the “non-template” method indicate that inter-fiber resistance can play a major role in reducing the conductivity to values as low as $\sim 10^{-2}$ S/cm [25]. In our studies, the 4-probe pressed-pellet room temperature DC conductivity was consistently in the range 1–5 S/cm regardless of doping percentage and/or fiber morphology. It is possible, however, that the high pressures used to prepare pellets for conductivity measurements might have destroyed the fibrillar morphology precluding any interfiber charge transport effects.

Polyaniline nanofibers are expected to have large accessible surface areas which could be potentially leveraged to advantage in capacitive charge storage applications [29]. The capacitance of polyaniline nanofibers increases as the fiber diameter decreases. Summarized in Table 1, a value of 277 F/g was observed for polyaniline-AMPSA (no

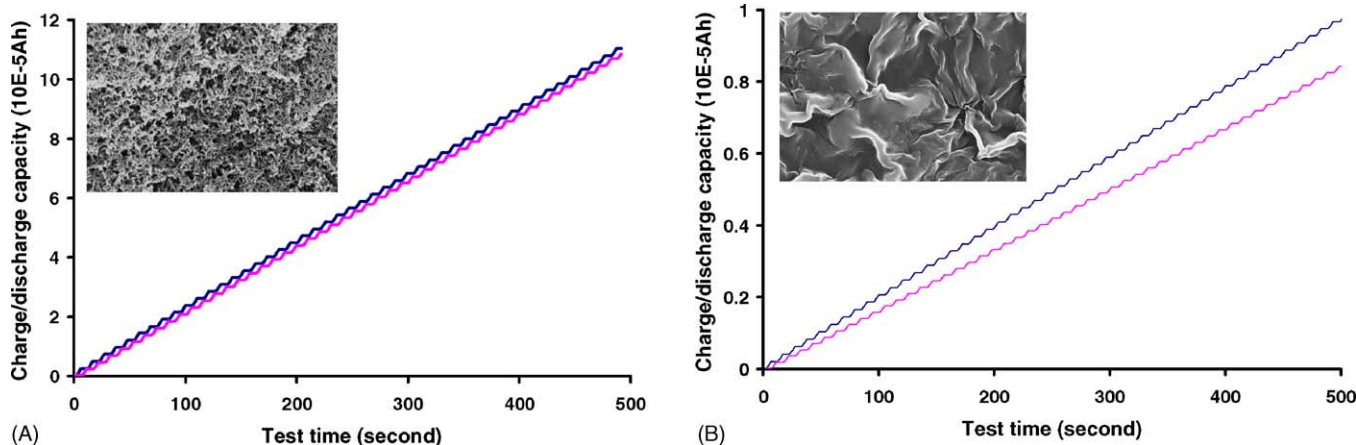


Fig. 4. Cumulative charge/discharge capacity of polyaniline-AMPSA (over 50 cycles) in the range 0.4–0.5 V (vs. SCE) in aq. 1.0M CSA electrolyte: (A) fibrillar morphology, average fiber diameter 23 nm [(0.1156 mAh \times 3.6)/(50 cycles \times 0.1 V \times 0.3 mg) = 277 F/g]; (B) non-fibrillar morphology [(0.0093 mAh \times 3.6)/(50 cycles \times 0.1 V \times 0.6 mg) = 11 F/g].

surfactant) nanofibers of average diameter 23 nm, in aq. 1.0 M CSA electrolyte in the potential range and 0.4–0.5 V (versus SCE). This potential range was chosen because it is in the “valley” between the two Faradaic (redox) peaks in the cyclic voltammogram (Fig. 3). Non-fibrillar polyaniline-AMPSA powder obtained from the same batch of polyaniline-AMPSA nanofibers using the dedoping/doping procedure outlined in Section 2 yielded a specific capacitance of approximately 11 F/g. A comparison of the charge/discharge capacities, over 50 cycles, between fibrillar versus non-fibrillar polyaniline-AMPSA is described in Fig. 4. It is clear that fibrillar morphology not only leads to significantly higher overall capacitance but also greater symmetry in the charge discharge cycles. Capacitance values were also estimated using the conventional “rectangular box” cyclic voltammogram plots (not shown) and these values compared favorably with the cumulative, composite charge/discharge plot shown in Fig. 4. In addition, the capacitance increases as the fiber diameter decreases which is also consistent with their larger surface areas. The unusually high capacitance of polyaniline-AMPSA could also be related to other factors, e.g., AMPSA is a “reactive dopant”, i.e., it could undergo free radical polymerization in aqueous oxidative conditions resulting in poly-AMPSA that could be playing a role in increasing the available surface area even further [30]. We have found solutions of aq. 1.0 M AMPSA containing ammonium peroxydisulfate to “gel” in a few hours.

4. Conclusions

Surface active dopants and/or surfactants allow some degree of control of fiber diameter in the synthesis of polyaniline nanofibers using the interfacial polymerization route. The influence of *cis*-1,2-ethenesulfonate family of twin-tailed surfactants on fiber properties has been described for the first time. While average fiber diameter can increase or decrease depending on the anion used to dope polyaniline, addition of twin-tailed surfactants always lowers the average doping percentage of polyaniline nanofibers. These high surface area nanofibers show promise in capacitive charge storage applications and in the development of next-generation energy storage systems.

Acknowledgements

We gratefully acknowledge helpful discussions with Dr(s). A.G. MacDiarmid, D.-S. Suh and for financial support

from The University of Texas at Dallas and University of Pennsylvania.

References

- [1] J. Huang, R.B. Kaner, *J. Am. Chem. Soc.* 126 (2004) 851; J. Huang, S. Virji, B.H. Weiller, R.B. Kaner, *J. Am. Chem. Soc.* 125 (2003) 314.
- [2] G.G. Wallace, P.C. Innis, *J. Nanosci. Nanotechnol.* 2 (2002) 441.
- [3] C.G. Wu, T. Bein, *Stud. Surf. Sci. Catal.* 84 (1994) 2269.
- [4] V. Misoska, W. Price, S. Ralph, G. Wallace, *Synth. Met.* 121 (2001) 1501.
- [5] V.M. Cepak, C.R. Martin, *Chem. Mater.* 11 (1999) 1363.
- [6] M.G. Han, S.K. Cho, S.G. Oh, S.S. Im, *Synth. Met.* 126 (2002) 53.
- [7] L. Yu, J.-I. Lee, K.-W. Shin, C.-E. Park, R. Holze, *J. Appl. Polym. Sci.* 88 (2003) 1550.
- [8] S.T. Selvan, *Chem. Commun.* 3 (1998) 351.
- [9] S.T. Selvan, J.P. Spatz, H.A. Klok, M. Moeller, *Adv. Mater.* 10 (1998) 132.
- [10] J.-E. Osterholm, Y. Cao, F. Klavetter, P. Smith, *Polymer* 35 (1994) 2902.
- [11] M.R. Simmons, P.A. Chaloner, S.P. Armes, *Langmuir* 11 (1995) 4222.
- [12] P.M. Beadle, S.P. Armes, S.J. Greaves, J.F. Watts, *Langmuir* 12 (1996) 1784.
- [13] M. Wan, Z. Wei, Z. Zhang, L. Zhang, K. Huang, Y. Yang, *Synth. Met.* 135–136 (2003) 175.
- [14] M. Wan, J. Li, *Polym. Adv. Technol.* 14 (2003) 320.
- [15] K. Huang, M. Wan, *Synth. Met.* 135–136 (2003) 173.
- [16] K. Huang, H. Qiu, M. Wan, *Macromolecules* 35 (2002) 8653.
- [17] T. Hatano, M. Takeuchi, A. Ikeda, S. Shinkai, *Chem. Lett.* 32 (2003) 314.
- [18] R.B. Read, C.Y. Meyers, L.R. Camp, R.C.Y. King, *Coal Prep.* 7 (1989) 85.
- [19] A.G. MacDiarmid, L.S. Yang, W.-S. Huang, B.D. Humphrey, *Synth. Met.* 18 (1987) 393.
- [20] S.K. Manohar, A.G. MacDiarmid, A.J. Epstein, *Synth. Met.* 41 (1991) 711.
- [21] F.M. Menger, J.S. Keiper, *Angew. Chem. Int. Ed.* 39 (2000) 1907.
- [22] L. Duic, M. Kraljic, S. Grigic, *J. Polym. Sci., Part A: Polym. Chem.* 42 (2004) 1599.
- [23] C.M. Randolph, A.J. McEvoy, *Phys. Chem.* 93 (1989) 905.
- [24] Y. Wei, Y. Sun, G.-W. Jang, X. Tang, *J. Polym. Sci., Part C: Polym. Lett.* 28 (1990) 81.
- [25] Y. Long, Z. Chen, N. Wang, Y. Ma, Z. Zhang, L. Zhang, M. Wan, *Appl. Phys. Lett.* 83 (2003) 1863.
- [26] A.G. MacDiarmid, J.-C. Chiang, W.-S. Huang, B.D. Humphrey, N.L.D. Somasiri, *Mol. Cryst. Liq. Cryst.* 125 (1985) 309.
- [27] J.E. Albuquerque, L.H.C. Mattoso, D.T. Balogh, R.M. Faira, J.G. Masters, A.G. MacDiarmid, *Synth. Met.* 113 (2000) 19.
- [28] J.Y. Shimano, *Synth. Met.* 119 (2001) 365.
- [29] W.-C. Chen, T.-C. Wen, H. Teng, *Electrochim. Acta* 48 (2003) 641.
- [30] T. Godjevargova, A. Dimov, *J. Appl. Polym. Sci.* 57 (1995) 487.